AD-A021 947

FAR INFRARED AND SUBMILLIMETER WAVE ATTENUATION BY CLOUDS AND RAIN

D. Deirmendjian

RAND Corporation
Santa Monica, California

April 1975

DISTRIBUTED BY:

NTIS
National Technical Information Service
U. S. DEPARTMENT OF COMMERCE

083144

AD-A021947

Far Infrared and Submillimeter

Wave Attenuation by Clouds and Rain

D. Deirmendjian

April 1975

DDC
RECEIVED
MAR 25 1976
A

P-5419

REPRODUCED BY
NATIONAL TECHNICAL
INFORMATION SERVICE
U.S. DEPARTMENT OF COMMERCE
SPRINGFIELD, VA. 22161

The Rand Paper Series

Papers are issued by The Rand Corporation as a service to its professional staff. Their purpose is to facilitate the exchange of ideas among those who share the author's research interests; Papers are not reports prepared in fulfillment of Rand's contracts or grants. Views expressed in a Paper are the author's own, and are not necessarily shared by Rand or its research sponsors.

The Rand Corporation
Santa Monica, California 90406

Far Infrared and Submillimeter Wave Attenuation by Clouds and Rain

ABSTRACT

Newly determined optical constants for water at far infrared and submillimeter wavelengths, as revealed by a recent survey, are used to estimate water cloud and rain attenuation over the wavelength range between λ1.2μm and λ2cm. For this purpose new analytic drop-size distribution models simulating fog, nimbostratus cloud, and rain corresponding to rainfall rates of 10 and 50 mm hr^{-1}, are set up. The corresponding volume extinction and absorption coefficients are computed according to polydisperse Mie scattering theory at specific wavelengths and presented in tables and graphically in plots for purposes of interpolation.

It is found that cloud extinction may exceed 50 nepers per kilometer in the λ≲100μm region whereas for wavelengths longer than λ200μm, under near saturated conditions, water vapor absorption should be the dominant attenuator. The greatest attenuation by heavy rain may be expected around λ5mm with a value of about 5 nepers per kilometer. The results also suggest that, in the presence of non-precipitating water clouds or fog there may be a relative transmission "window" centered around λ1.3 mm.

ACCESSION for
NTIS
DDC
BY
DISTRIBUTION/AVAILABILITY CODES

ADDENDUM

P-5419 FAR INFRARED AND SUBMILLIMETER WAVE ATTENUATION BY CLOUDS AND RAIN, by D. Deirmendjian, April 1975.

Please add the following as a footnote referring to the word "(neper)" appearing on line 5, p. 15.

*As used here and elsewhere in this paper, the term "neper" refers to units of the exponential attenuation of power or energy flux, rather than of amplitude or voltage as in accoustical and electrical engineering usage.

PUBLICATIONS DEPARTMENT

Rand
SANTA MONICA, CA. 90406

1. Introduction

In earlier work we introduced a set of continuous size distribution models to simulate natural atmospheric particulates such as aerosols or haze, cloud droplets, and raindrops to deduce their single scattering and absorption properties (Deirmendjian, 1963a,1964, 1965, 1969). These models have been found useful in various application by other authors. The work covered the visible and infrared spectrum between the wavelengths of λ0.45 and λ16.0 μm, and the microwave spectrum between λ1 mm and λ8 cm where reasonably accurate data on the optical constants of water--the main constituent of atmospheric particles--were available. As is well known, the extinction and scattering properties of individual particles (van de Hulst, 1957) as well as of polydispersions (Deirmendjian, 1969) depend critically on the optical constants, i.e., the real and imaginary parts of the refractive index, of the particle substance with respect to the ambient medium.

Two recent developments make it possible and desirable now to consider the far infrared and submillimeter region between λ10 μm and λ1000 μm: The advent of several types of new maser sources of monochromatic radiation within the region (Fox, 1971; Button, 1974) and the publication of new experimental results on the far infrared optical constants of water as revealed by a recent survey (Deirmendjian, 1974). There is no doubt that these new sources will find many applications, some of which will be related to the terrestial atmosphere either as a subject of direct study or as a disturbance interposed between source and receiver. Electro-

magnetic wave scattering, is connected to both aspects: as a diagnostic of particulates through the study of the directional variation of scattered intensity and its polarization, and as an attenuating disturbance through the absorption and scattering cross-section of the particles. As is well known, the most efficient scattering is produced by a particle whose linear dimensions are of the order of the wavelength of the incident radiation. Cloud and rain particles have typical diameters of tens and hundreds of micrometers which are just right for maximum interaction with *far infrared* ($15 \lesssim \lambda \lesssim 100$ μm) and *submillimeter* ($100 \lesssim \lambda \lesssim 1000$ μm) waves.

The present paper covers mainly the attenuation properties of these hydrometeors leaving the directional scattering and polarization properties for a projected separate study. In particular, we shall first introduce and justify some new cloud and rain drop size distribution models developed for use in this study. We then present the results of attenuation calculations for these models for selected wavelengths and optical constants using polydisperse Mie scattering theory and computer programs developed earlier (Deirmendjian, 1969). Finally we analyze and compare our estimates with other work and with observation, where possible, and discuss some implications in atmospheric applications.

2. The optical constants of liquid water

It is well known that the behavior of the optical constants or real and imaginary parts ν, and κ, respectively, of the index of refraction $m \equiv \nu - i\kappa$, for liquid water is rather complex. Particularly in the middle and far infrared region, both parts are highly frequency-dependent and vary

considerably with temperature in a nonlinear, nonmonotonic way.

Numerous experimental and theoretical techniques and models are used in evaluating these so-called constants. Here we shall merely mention some of the original published sources we have used in the present work referring the reader to a longer survey for more details (Deirmendjian, 1974).

The complex index of refraction m (with respect to free space) is usually defined either in terms of Maxwellian electromagnetic theory as the square root of a complex dielectric constant or a generalized Snell's law, provided the angle of refraction in a lossy medium is also defined as a complex number. In either case, the real part, ν may be related to changes in the wave's phase angle, speed, and direction of propagation upon entering the medium from free space; and the imaginary part, κ, to the bulk absorption cross-section, γ_b, per unit volume within the medium, through the relation

$$\kappa = \frac{\gamma_b \lambda}{4\pi} \tag{1}$$

where the wavelength λ and γ_b involve mutually reciprocal units so that κ is nondimensional. For weakly absorbing or "transparent" media the real part may be obtained experimentally by an appropriate application of Fresnel's generalized formulas for reflection and refraction. This method, of course, is not practical for water in the far infrared because of its quasi metallic behavior in its optical properties, and other experimental and analytical tools must be devised.

In principle the imaginary part, κ, may be obtained experimentally for example by use of Beer's law by measuring the absorption through a

variable thickness of the material. In practice, however, because of the very high infrared absorptivity of water one has to use a very small thickness--of the order of a few wavelengths--of the sample which presents considerable experimental and analytical difficulties.

The optical behavior of liquid water varies greatly throughout the spectrum, from that of a transparent dielectric in the visible to a metallic type in the far infrared region. Some of the difficulties in measuring the far infrared optical constants have been overcome by a combination of experimental data and theoretical models. A brief description of these methods is given in the above mentioned survey (Deirmendjian, 1974) together with an intercomparison and critique of their reliability. Here we shall merely summarize the results of the survey and list the values actually used in our calculations.

Our survey indicated that the optical constants of water in the middle and far infrared below about $\lambda 40$ μm are fairly well determined. At longer wavelengths there are uncertainties, particularly in the refractive index, and in the temperature dependence of both the index and the absorption coefficient. It is possible to propose a set of most probable values, based on the latest measurements at room temperature, which are adequate for purposes of scattering calculations. The results of our survey are conveniently summarized by the points and curves of Fig. 1 plotted on logarithmic scales for both the wavelength and the optical constants. The ordinate serves a double purpose: the left-hand scale is marked in units of the imaginary part κ, of the complex index; the right-hand scale is marked in units of $(\nu - 1)$ for convenience of representation.

The continuous curves are plots of the smoothed values proposed and tabulated by Hale and Querry (1973) and based mostly on work by a Kansas State University group initiated by Dudley Williams and his collaborators (Draegert et al, 1966). In Fig. 1, the solid curves for water ending at $\lambda 50$ μm show their "best" values and should be regarded as fairly illustrative--but not definitive--for the region. At longer wavelengths, their tabulations, indicated by the dotted curves ending at $\lambda 200$ μm, may be less reliable and subject to future correction.

The open dots in Fig. 1 represent the optical constants adapted from the data of Davies et al. (1970) in the region $100 \leq \lambda \leq 1600$ μm. In general we believe that these values represent the most reliable data within their range of coverage. In the millimeter region, the Davies et al. (1970) experimental values at $\lambda 1$ mm compare very well with those given by the Debye formula as adapted for example by Ray (1972) for water at 30°C.

For completeness and comparison we have included in Fig. 1 the optical constants for ice according to some recent data (Deirmendjian, 1974), in the same manner as those for water. The continuous curves follow the tabulations for ice I at -7° by Schaaf and Williams (1973)(see labels and legends on the diagram). The dashed lines connecting open triangles indicate the tabulations of Bertie et al. (1969) for ice I at -173°C. This temperature is well below the atmospheric temperatures of cirrus cloud particles and snow. An extrapolation with respect to temperature is not possible with present knowledge. Furthermore, atmospheric ice particles are mostly nonspherical and irregular in shape, and a scattering theory for such particles of finite size with respect to the wavelength does not exist except for inapplicable approximations. Hence the attenuation

of far infrared and submillimeter radiation through cirrus clouds and snow can be obtained only as a rough estimate for which an exact knowledge of optical constants is not essential.

It appears that, despite experimental difficulties, the optical constants for liquid water--at least at room temperature or 24°C--are fairly well determined in the entire range up to millimeter waves. At atmospheric temperatures near 0°C, their values may be smaller than shown in Fig. 1 by an unknown amount of the order of a few percent. However because of mutually compensating effects of such changes on the scattering efficiencies of the smaller and larger particles in a polydisperse aggregate, the error in the overall extinction coefficient may not be significant if the room temperature data are used.

For convenience we show in Table 1 the actual wavelengths we chose for our calculations together with the corresponding complex index values as adapted from the original data summarized in Fig. 1. A higher spectral resolution is not necessary in view of the expected smooth variation of polydisperse scattering attenuation with wavelength. For wavelengths in excess of λ2 mm we used the Debye formula values as in an earlier study (Deirmendjian, 1965) valid for 0°C water. In the $28 \lesssim \lambda \lesssim 1000$ μm spectral region, the optical constants shown are valid for room temperature or 24°C, as obtained by experiment, even though cloud and raindrops are certainly at a lower temperature. Since the temperature dependence of these constants seems to be uncertain at present we shall use the 24°C values here without further adjustment.

3. Extinction coefficient for polydispersions

The theory of polydisperse scattering to be used may be outlined as follows. Let the number density of cloud or rain drops in a typical volume of air be given by a continuous function $n(r)$, where r is the radius of the spherical particles. Then, if $\sigma_{ex}(m,r)$ is the extinction (scattering + absorption) cross section as a function of r and the optical constants ν and κ, where $m \equiv \nu - i\kappa$ is the complex index of refraction, it can be shown that

$$\beta_{ex}[\lambda,m,n(r)] = \int_{r_1}^{r_2} \sigma_{ex}(m,r)n(r)dr \qquad (2)$$

is the *volume extinction coefficient*, β_{ex}, for the polydispersion, where r_1 and r_2 are the lower and upper limits in the droplet radius r, and λ is the central wavelength of the incident radiation. This may consist of a narrow band of incoherent unpolarized radiation or a coherent, monochromatic wave train, provided that the distance between drops is large with respect to λ and that the drops' space distribution is random and nonstationary.

It is well known that, for spherical particles of finite size with respect to λ, the behavior of σ_{ex} is highly dependent on r and m. In the exact theory (see e.g. van de Hulst, 1957) one defines an extinction efficiency or normalized cross section $K_{ex}(m,x) \equiv \sigma_{ex}/(\pi r^2)$, given by a so-called Mie series whose terms contain ratios of Ricatti-Bessel functions of real or complex argument involving the normalized size $x = 2\pi r/\lambda$ and m. These series can be readily evaluated using appropriate programs for high-speed data processing systems (see e.g., Deirmendjian, et al, 1961; Deirmendjian, 1969). Thus the extinction integral in (2), after a change

of variable, takes the form

$$\beta_{ex}(\lambda,m,n) = \pi\left(\frac{\lambda}{2\pi}\right)^3 \int_{x_1}^{x_2} x^2 n(x) K_{ex}(m,x)dx. \qquad (3)$$

From (3) it is clear that for polydispersions containing mainly finite particles with respect to the wavelength, β_{ex} is critically dependent on the form and magnitude of n(x), the size and size-range of the particles, as well as on their optical constants.

Two limiting cases are worth recalling: the geometric optics or large sphere approximation with $\lambda << r$; and the long wave (low frequency) or small particle approximation, with $r << \lambda$, where the shape of the particle is unimportant. In the first case, provided the spheres are lossy and $\kappa \neq 0$, it is well known by physical argument (van de Hulst, 1957) and mathematical treatment of the Mie series (Chýlek, 1973) that $x \to \infty$ limit of K_{ex} is 2. Hence if *all* the particles in the polydispersion are in the geometric optics domain, we have the well known result that β_{ex} is given by

$$\beta_{ex}[n(r)] = 2\pi \int_{r_1}^{r_2} r^2 n(r)dr, \qquad \lambda << r; \qquad \kappa \neq 0 \qquad (4)$$

or twice the sum of the geometrical cross-sectional areas of all the particles in a unit volume. Clearly the value of β_{ex} in this case is independent of the wavelength and the optical constants but very much a function of the density distribution n(r). In the nonabsorbing case, where $\kappa = 0$, the $x \to \infty$ limit of the scattering or extinction cross section does not exist, as conjectured by Deirmendjian (1969) and rigorously demonstrated by Chýlek (1973), and the integration (4) is not valid. However, since we are dealing with the infrared spectrum where liquid water always shows some absorption, this question is not of concern here.

In the other limit, a small particle approximation for the extinction efficiency may be given as a power series in the size parameter x (van de Hulst, 1957; Penndorf, 1962). In particular, as shown by Deirmendjian (1963b) use of the first term in x in such a series, equivalent to setting

$$K_{ex}(m,x) = \frac{24\nu\kappa}{Z}\, x, \qquad x \ll 1, \tag{5}$$

where

$$Z \equiv (\nu^2+\kappa^2)^2 + 4(\nu^2-\kappa^2+1),$$

may be sufficient, provided κ is not small compared to 1 and $x \lesssim 0.01$. Expression (5) represents also the absorption efficiency K_{ab} in the Rayleigh approximation, in which case $K_{ab} \to K_{ex}$, $K_{sc} \to 0$ for any value of κ no matter how small, provided x is sufficiently small (Deirmendjian, 1969). The extinction cross section itself may be obtained from (5) in terms of the volume v occupied by the particle, that is by writing

$$\pi r^2 K_{ex} = \sigma_{ex} = \frac{36\pi\nu\kappa}{Z}\,\frac{v}{\lambda} \quad . \tag{6}$$

The extension of this result to a polydispersion follows easily by substituting (6) into (2) to obtain

$$\beta_{ex} = \beta_{ab} = \frac{36\pi\nu\kappa}{Z}\,\frac{1}{\lambda}\,V_p, \qquad r_2 \ll \lambda \quad , \tag{7}$$

where

$$V_p \equiv \frac{4}{3}\pi \int_{r_1}^{r_2} r^3 n(r)dr$$

is the volume of all the particles in the polydispersion per unit volume of space. Note that (7) is strictly valid only when the largest particle r_2

is itself much smaller than λ, but this restriction may be relaxed depending on the nature of the density function n(r). From (7) it follows that in this limiting case the form of the density function does not affect the extinction if the volume mixing ratio V_p remains constant.

4. Drop-size distribution functions

For the size distribution function we shall use the general form

$$n(r) = a\, r^{\alpha} \exp\,(-br^{\gamma}) \tag{8}$$

first used by this author[1] to model both clouds and hazes, as well as raindrops (Deirmendjian, 1963a,b). This function vanishes for very small and large radii and has a single maximum. The constants a, α, b, and γ are real positive numbers that may be related to measurable parameters. For example, for the special case $\gamma = 1$, it can be easily shown by integration of (8) between $r = 0$ and ∞ that

$$a = N \frac{b^{\alpha+1}}{\Gamma(\alpha+1)}, \quad \gamma = 1, \tag{9}$$

where N is the total number of particles per unit volume in the distribution. Similarly the constant b is given by the mode radius r_c or size of greatest frequency by means of the relation $b = \alpha/r_c$. (We note that Hansen (1971) has recently introduced a distribution function which is identical to (8), except for a redefinition of the constants in terms of other quantities, without additional physical justification in our opinion. The conversion from one set of constants to the other is easily derived by comparing the two forms.)

---

1 Green and Lane (1964) cite a 1939 paper by S. Nukiyama and Y. Tanasawa who found that this identical function represents the size distribution of droplets produced by "small air blast atomizers".

Among the desirable properties of the form (8) is the exponential decay in number density with increasing drop size. This and the nature of the Mie functions result in a rapid convergence of the integrals of type (3) in the region defined by the condition

$$r_2 > \frac{\alpha+4}{b}, \ \gamma = 1 \tag{10}$$

where r_2 is the radius corresponding to the upper limit x_2 of integration. This behavior closely corresponds to natural atmospheric polydispersions where there is a cutoff of the distribution at the upper end due to various processes. The function (8) also vanishes for very small r due to the power factor, again corresponding to natural conditions, so that the integral (3) may be replaced by a definite one between the limits 0 and ∞ without loss of applicability.

In the past our H, L, and M haze models, and C.1 cloud model for fair weather cumulus have been found useful in various applications of radiative transfer theory to problems related to the atmospheres of the earth and Venus (see, e.g., Hansen, 1971; Thompson and Wells, 1971; Hansen and Hovenier, 1974; Kattawar and Plass, 1975). Obviously the mode radius of 4 μm in the C.1 model is too small and the drop size range too narrow to simulate a precipitating type cloud. We shall now introduce two new cloud density functions to simulate fog or nimbostratus, called *cloud C.5*, and a large droplet component, called *cloud C.6*. These choices have been mainly suggested by measurements, such as Okita's (1961), and others, taken within clouds that are producing precipitation. A

more detailed discussion and justification is deferred to a planned separate paper.

The specific form of our cloud C.5 density function is

$$n(r) = a\, r^4\, e^{-2r/3}\ \mathrm{cm}^{-3}\ \mu\mathrm{m}^{-1}, \tag{11}$$

with a mode radius of r_c of 6 μm. For a nominal density of N = 100 droplets per cm^3, this model shows a liquid water content w of 0.297 g m^{-3}. It is interesting to note that Hansen's (1971) "mean effective radius" of 10.5 μm and "effective variance" of 0.143, corresponding to our C.5 distribution, coincide almost exactly with those of Diem's measured distributions for cumulus congestus and nimbostratus clouds as reduced by Hansen (*op. cit.*).

For cloud C.6 we adopted the formula

$$n(r) = a\, r^2\, e^{-r}\ \mathrm{cm}^{-3}\ \mu\mathrm{m}^{-1} \tag{12}$$

with r_c = 20 μm. For a typical density of 10^{-1} drop per cm^3, this model shows a water content of 0.025 g m^{-3}. A simple sum of the density functions (11) and (12) reproduces fairly well two of Okita's (1961) droplet spectra (for August 19, 1958) measured within a nimbostratus cloud. Their liquid water contents are given as 0.33 and 0.46 g m^{-3} respectively which compare well with our models' 0.322 g m^{-3}.

In general, the modeling of cloud drop spectra is relatively straightforward, since clouds usually are fairly stable for the purposes of droplet counting and sizing by modern instrumentation. The phenomenon of rain, on the other hand, represents highly unstable conditions so that it is difficult to define a raindrop density function without specifying several pertinent variables and meteorological conditions for each case. The easily recorded rainfall rate, R, is an integral over most such variables, and its dependence on droplet growth and breakup, fall velocities and updrafts, distance below cloud, etc., is not well known. Nevertheless,

any extinction of electromagnetic flux by rain must be interpreted in terms of the "instantaneous" (really some sort of time and space average) drop-size distribution encountered by the beam. In radar meteorology these questions are usually bypassed by the adoption of the so-called "Z-R" empirical relations that seem to work in operational situations (Battan, 1973).

Here we shall introduce two raindrop density functions of the type (8) as examples of moderate and heavy rainfall conditions, as suggested by some recent drop-size distribution and simultaneous rainfall rate measurements. Our moderate rainfall model, called *rain-10*, is designed to represent drop spectra just below the cloud base when a precipitation rate of about 10 mm hr^{-1} is measured at the ground. The corresponding density function is

$$n(r) = a\, r^4\, e^{-12r}\ m^{-3}\ mm^{-1}, \tag{13}$$

where $r_c = 1/3$ mm. The constant a is fixed for a nominal N = 1000 drops per m^3 and a liquid water content of 0.509 g m^{-3}. Note that the model (13) distribution differs from the one we introduced earlier (Deirmendjian, 1969), called rain L (for light rain aloft), notably in the choice of a bigger mode radius, for better agreement with Doppler radar data.

Our heavy rain model, called *rain-50*, is designed to represent raindrop spectra at ground level during rainfall rates of the order of 50 mm hr^{-1}. Its density function is given by

$$n(r) = a\, r^6\, e^{-10r}\ m^{-3}\ mm^{-1} \tag{14}$$

where $r_c = 0.60$ mm, a is fixed for N = 1000 drops per m^3 and w = 2.11 g m^{-3}.

The two models are illustrated by the solid continuous curves in Fig. 2, labeled "Rain-10" and "Rain-50". For comparison, one of the Doppler measurements obtained by Caton (1966) corresponding to a measured rate of 5.6 mm hr^{-1} and two of the ground-level measurements from Cataneo and Stout (1968) are also indicated on Fig. 1 by the labeled broken curves. Although the agreement is not perfect, our models are seen to be fairly representative of these particular measurements.

We emphasize that the above cloud- and raindrop size spectral models are introduced to evaluate the far infrared and submillimeter wave attenuation to be expected in typical cases. They are not intended as a detailed discussion of drop spectra and their relation to cloud microphysics. We do suggest, however, that linear combinations of these models, together with those of the same type we introduced in earlier work, are capable of reproducing many of the naturally occuring water drop spectra and the resulting scattering properties.

5. The extinction coefficients for clouds and rain

The polydisperse extinction coefficients were computed on an IBM 370/158 system for the models described in Sec. 4 at the wavelengths and optical constants of Table 1 by the numerical techniques described previously elsewhere (Deirmendjian, 1963a, 1969). The problem of computational instabilities in the evaluation of Bessel functions of large complex argument was overcome without difficulty by using the double precision arithmetic and forward recursion techniques already described *(op. cit.)*.

Selected values of β_{ex} and the *volume absorption coefficient* β_{ab} (obtained by an integral similar to (3), are listed in Tables 2 and 3. The difference, $\beta_{ex} - \beta_{ab} = \beta_{sc}$, is the *volume scattering coefficient*, as defined in radiative transfer formulations. The conventional units of (neper) km^{-1} shown, should really be interpreted as a cross-sectional area per unit volume, or in this case as $cm^2(10^5 cm^3)^{-1}$, such that the attenuated flux F of a plane-parallel or collimated stream of electromagnetic energy is given by

$$F = F_o \exp \left\{-\beta_{ex} L\right\} \tag{15}$$

where F_o is the source energy and L is the path length in kilometers through a homogeneous scattering medium. In Tables 2 and 3 the numbers shown in parentheses were obtained by approximations (4) and (7), as the case may be. The definite integrals involved in these approximations may be easily evaluated from their analytic expressions in terms of gamma functions, after substituting the explicit forms for n(r) in each case and integrating between the limits $r = 0$ and ∞.

For the limits $x_1(\lambda, r_1)$ and $x_2(\lambda, r_2)$ of the numerical integration (3), we used the criterion that $n(r_1)$ and $n(r_2)$ should be less than $10^{-3} n(r_c)$, where $n(r_c)$ is the maximum of the density function. The upper limit in this case is also governed by the condition $r_2 > 2(\alpha+4)/b$, that is twice the value beyond which rapid convergence is assured according to (10). The integration steps were varied for each case to assure good accuracy without wasting machine time. The values shown in Tables 2 and 3 should be accurate to the four significant figures indicated.

The extinction coefficients in Tables 2 and 3 are displayed graphically in Fig. 3 where they are plotted as solid dots logarithmically against the wavelength. This is marked in micrometers and millimeters on the lower scale and the corresponding frequency in GHz units or 10^9 sec^{-1} is indicated on the top scale. The ordinate scale on the left shows the extinction coefficient in nepers per kilometer and on the right-hand scale in decibels per kilometer for convenience (conversion factor nepers to decibels: 4.343). The curves are fitted "by eye" to the data points and their dashed extensions connect the small particle approximations shown in parentheses in Tables 2 and 3. The dashed straight lines with arrows pointing to the left are the asymptotic values for large spheres according to (4). For completeness and comparison we also extended the extinction evaluations of our original fair weather cumulus or cloud C.1 model (Deirmendjian, 1963a, 1969) to the far infrared with the use of the new optical constants shown in Table 1. (The C.1 model has a mode radius r_c of 4 μm and a water content of 0.063 g m^{-3} for a drop density of 100 cm^{-3}.) The resultant infrared and submillimeter extinction curve is included in Fig. 3 fitted to the values listed in Table 2.

Tables 2 and 3 list the volume extinction and absorption coefficients for normalized *number* densities corresponding to the various models and may be used to scale these coefficients to other number densities as given by observation or equivalent theoretical models. It is convenient and instructive to also consider the extinction coefficient per unit *mass* of particles. This is easily derived from the tables in terms of

the number of particles N_m per unit volume, per unit mass of substance. From the volume mixing ratio V_p in (7) and the integrated number density N as in (9), we have

$$N_m = \frac{N}{\rho V_p} \tag{16}$$

where ρ is the density of the particle substance. In the case of water clouds and hazes, the *liquid water content* $w = \rho V_p$, usually expressed in grams per cubic meter, may be obtained from (16) by expressing V_p in cm^3 per m^3 with $\rho = 1$ in which case $w = 10^6 V_p$. Consequently $10^{-6} N_m$ represents the number of particles per unit volume per g m^{-3} of liquid water content and the mass extinction coefficient, γ_{ex}, is obtained from β_{ex} by writing

$$\gamma_{ex}[n(r),w] = 10^{-6} \frac{N_m}{N} \beta_{ex} = w^{-1}\beta_{ex}. \tag{17}$$

In Table 4 we list sample values of the mass extinction coefficients for two of our cloud models, C.1 and C.5, the rain model rain-10, and for comparison our original haze model L (r_c = 0.07 μm) corresponding to a continental type distribution (Deirmendjian, 1969). The use of parentheses in Table 4 has the same meaning as in Tables 2 and 3. The reader can derive other values by use of equation (17) and the liquid water contents for each model. These values may be used to scale the extinction of clouds and rain for liquid water contents other than those adopted in our models, *provided that the size distribution can be approximated by these models.* In fact, as is clear from Table 4, for a given water content the amount of extinction produced by water particles depends very much on their relative size and number distribution.

Compare for example the $\lambda \to 0$ values, characteristic say of $\lambda 0.70$ μm or visible light, for rain and haze where there is a thousandfold increase in extinction per unit mass of liquid water. The mass extinction coefficient at any given wavelength becomes independent of size only when all the particles in the distribution are small compared to the wavelength as follows from equation (7).

6. Discussion and conclusions

As may be seen from Tables 2 and 3 and Fig. 3, the highest extinctions should be observed in nimbostratus-type clouds (or fog) at $\lambda < 200$ μm. Here the computed extinction coefficients may even be underestimated by factors of two or three considering that real clouds may contain 200 to 300 droplets per cm^3 (Mason, 1971). However, beyond $\lambda 100$ μm the cloud extinction values fall more or less as λ^{-1} and are exceeded by those for moderate rain at millimeter wavelengths.

A comparison of the extinction curves for the fair weather cumulus C.1 and stratus cloud C.5 shows them to be approximately parallel, both showing the relative "window" in the $10 \lesssim \lambda \lesssim 12$ μm region. At shorter wavelengths toward the visible the extinction ratio $\beta_{ex}(C.1)/\beta_{ex}(C.5)$ is given by that of the asymptotic values for $\lambda \to 0$ listed in Table 2, that is, 0.37, which is also the ratio of the corresponding integrated geometric cross sections (4). At wavelengths longer than $\lambda 1$ mm the same ratio is seen to be 0.21, which is exactly that of the water contents of the two models. The contribution of cloud C.6, as expected, is seen to be quite small compared to those of the other models except in the region $\lambda > 100$ μm where it is of the same order as the cloud C.1 extinction.

In the real world, of course, the extinction by clouds may vary considerably--though not by an order of magnitude--from the estimates given here, depending on the cloud type, water content, homogeneity, etc. Our estimates are for illustrative purposes only and do not include, for example, the very important contribution by the strong water vapor absorption bands known to exist in the entire region. Although this subject is not within the scope of this paper, we note that, according to theoretical estimates (Birch et al, 1969), the H_2O absorption may exceed the cloud drop extinction.

The rain extinction curves are quite smooth and approach their asymptotic values quickly for wavelengths shorter than 100 μm or so. At the other end of the spectrum, note from the last line in Table 3 that at λ3.3 cm the ratio 7.68 of the extinctions for the rain-50 and rain-10 models differs significantly from that of their respective water contents, namely 2.11/0.509 = 4.15. This demonstrates that the small sphere approximation (7) is not good enough at this wavelength, as pointed out elsewhere (Deirmendjian, 1963b). The maximum in rain extinction occurs somewhere between λ2 and λ5 mm for both models, in a region where the cloud effect is small and dropping rapidly toward longer waves.

A rough comparison of our rain extinction estimates with independent evaluations may be obtained by graphical interpolation on data adapted from the literature by Dudzinsky (1974). For a rainfall rate of 50 mm hr^{-1}, our value and that estimated by D. E. Setzer (Dudzinsky, 1974, Fig. 1) coincide exactly at λ10 mm, while at λ33 mm our value is somewhat lower than Setzer's estimate. Similarly, our rain-50 model values fall

between the "world" measured maximum and minimum attenuations as given by R. G. Medhurst and summarized by Dudzinsky (1974, Fig. 3). For wavelengths shorter than λ5 mm there seem to be few, if any, observations and our present theoretical values may be useful in the design of future experimental programs and applications.

For the cloud extinction values in the submillimeter region also there are few independent estimates and experimental values to allow a comparison. A good determination, on the basis of a series expansion of K_{ex}, is provided by Platt (1970). Platt made use of the first three terms of the power series in x, instead of only the first, as in equation (5), to obtain the extinction contribution from the larger droplets at λ200 and λ337 μm, his two shortest wavelengths, together with the best optical constants available to him. We compare below his determinations for a typical fog distribution with our own model values from Table 4, expressed in units of nepers per kilometer per unit liquid water content:

	λ 200 μm	λ 337 μm
Platt (1970, Table 5)	21.4	9.46
Cloud C.1 (N_m = 1599)	15.6	9.29
Cloud C.5 (N_m = 337)	18.9	9.93

Considering the differences in method and drop-size distribution, the agreement is quite good, especially at the longer wavelength as expected, and corroborates Platt's (1970) method of approximation in these cases.

Finally a comparison with available measurements of attenuation in the natural atmosphere should be made as a check of the validity of our models. Unfortunately there are too few published measurements, over a wide enough portion of the far infrared spectrum, for an adequate comparison. The point marked "Fog (obs)" on Fig. 3 is adapted from a determination at the HCN maser wavelength of λ337 μm (Burroughs et al, 1966) obtained in fog with a visibility of 35 m. This is equivalent to an extinction coefficient of about 96 nepers per kilometer at visible wavelengths according to a modification of Koschmieder's formula (Middleton, 1952), or about double the short wave asymptotic value for our cloud C.5 model. This implies that the fog contained some 200 droplets per cm^3 and a liquid water content of about 0.6 g m^{-3}, not at all unreasonable numbers according to existing measurements (Mason, 1971). Our corresponding extinction coefficient at λ337 μm from Table 2 or 4 is 5.9 km^{-1} which checks very well with the Burroughs et al. (1966) measurement of 5.8 km^{-1} plotted on Fig. 3 and constitutes a kind of validation of our model to represent some fogs.

The point on Fig. 3 marked "water vapor (obs)" is adapted from the same source. It represents a water vapor absorption equivalent to an attenuation of 11.5 km^{-1}, measured over a horizontal path, indicating the magnitude of this component in clear air in the absence of fog and with an absolute humidity of 4.84 g m^{-3}. Within precipitating clouds or fog under saturation conditions, the absolute humidity may be of the order of 10 g m^{-3} with a corresponding increase in water vapor absorption.

An idea of the magnitude of attenuation to be expected under extreme conditions of both fog and heavy rain in the path of a beam of λ337 μm radiation is given by the crossed circle on Fig. 3, marked "total estim.," arrived at as follows:

	Nepers km^{-1}	Decibels km^{-1}
H_2O absorption (10 g m-3)	24.0	104.
Cloud C.5 ($w = 0.6$ g m^{-3})	5.90	25.6
Cloud C.6	0.68	2.95
Rain-50	4.06	17.6
Total	34.64	150.2

In this example we see that rain accounts for only about 12 percent of the total, the heaviest contribution being that of water vapor absorption.

As to attenuation by other types of cloud and precipitation composed of ice particles, snow, and hail, an accurate theoretical estimate is unobtainable at present, since (a) the effects of the irregularity of their shape are not well known except for highly idealized models, and (b) the optical constants for ice in the submillimeter region have so far been determined only for unrealistically low temperatures. However, a rough idea of the attenuating properties of such particles could be obtained in certain cases by using the applicable asymptotic approximations discussed earlier.

The scope of the present study should be sufficient to provide good estimates of the attenuating effects of terrestrial water clouds and rain for wavelengths up to λ20 mm. Our results apply only to

power degradation due to incoherent scattering but not to phase and coherence losses caused by other types of scattering and turbulence. Water vapor absorption under atmospheric conditions needs further study. There seem to be several window-like bands in the region $0.83 \lesssim \lambda \lesssim 8.6$ mm, according to papers presented in two recent symposia (Fox, 1971; Button, 1974) based on theoretical estimates and laboratory determinations. From our present results it would thus seem that, in the presence of nonprecipitating water clouds, the presence of a relative "window" around $\lambda 1.3$ mm or a frequency of 230 GHz might be postulated. At this frequency Wrixon (1974) obtained a fairly good estimate of the "clear sky" zenith attenuation, of about 1 dB or an optical thickness of 0.23, by using the reliable Bouguer-Langley method and solar millimeter radiation. This is of the same magnitude as that of 1 km of cloud C.1. Precipitating type clouds, fog, or rain, however, would increase the value by large factors depending on their thickness and direction of "line of sight".

We, of course, have also generated the angular scattered intensity and polarization parameters corresponding to the new cloud and raindrop density models introduced here. Their analysis and implications in cloud microphysics research will be discussed in separate papers.

Acknowledgements. The kind assistance of the late Dr. John Chamberlain of the British National Physical Laboratory, Teddington, in making available his prepublication laboratory results is gratefully acknowledged. The initial research and computations were partly supported under the U. S. Air Force Project RAND.

Table 1

WAVELENGTH AND COMPLEX INDICES OF REFRACTION

λ	m	λ	m
12.μm	1.111 - 0.199i	500.μm	2.22 - 0.740i
17. "	1.376 - 0.429i	700. "	2.32 - 0.890i
28. "	1.549 - 0.338i	1000. "	2.50 - 1.09i
40. "	1.519 - 0.385i		
60. "	1.703 - 0.587i	2.mm	2.5604 - 0.8947i
100. "	2.06 - 0.551i	5. "	3.1918 - 1.7657i
140. "	2.07 - 0.470i	10. "	4.2214 - 2.5259i
200. "	2.08 - 0.509i	20. "	5.8368 - 3.0046i
357. "	2.20 - 0.600i	33. "	7.1755 - 2.8642i

Table 2

CLOUD VOLUME EXTINCTION AND ABSORPTION COEFFICIENTS

(Neper km^{-1})

λ	Cloud C.1 ($N=10^2 cm^{-3}$)		Cloud C.5 ($N=10^2 cm^{-3}$)		Cloud C.6 ($N=10^{-1} cm^{-3}$)	
	β_{ex}	β_{ab}	β_{ex}	β_{ab}	β_{ex}	β_{ab}
($\lambda \to 0$)	(15.64)		(42.41)		(0.7540)	
12. μm	10.28	7.352	36.32	22.61	0.7933	0.4030
17. "	16.12	10.23	49.98*	28.49*	0.8500*	0.4113*
28. "	12.33	7.849	49.88	27.36	0.9004	0.4521
40. "	8.468	6.392	39.86	24.89	0.9250	0.4774
60. "	7.013	5.816	37.69	25.41	0.9742	0.5065
100. "	2.690	2.415	20.70	14.55	1.061	0.553
140. "	1.420	1.352	9.742	7.797	1.074	0.555
200. "	0.9732	0.9570	5.617	5.109	0.9774	0.5190
337. "	0.5812	0.5789	2.949	2.880	0.6845	0.4016
500. "	0.4566	0.4560	2.235	2.219	0.4186	0.2911
700. "	0.3474	0.3472	1.676	1.671	0.2563	0.2031
1000. "		(0.2423)	1.165	1.164	0.1440	0.1274
2. mm		(0.0999)		(0.474)		(0.0401)
5. "		(0.0381)		(0.181)		(0.0153)
10. "		(0.0119)		(0.0563)		(0.0048)

*Values from an earlier run with m=1.369-0.438i

Table 3

RAIN VOLUME EXTINCTION AND ABSORPTION COEFFICIENTS
(Neper km^{-1}, $N=10^3 m^{-3}$)

λ	Rain-10		Rain-50	
	β_{ex}	β_{ab}	β_{ex}	β_{ab}
(λ→0)	(1.310)		(3.519)	
60.μm	1.396	0.598		
100. "	1.434	0.607	3.770	1.566
140. "	1.462	0.635		
200. "	1.502	0.666	3.905	1.677
337. "	1.577	0.715	4.062	1.766
500. "	1.651	0.769	4.218	1.868
700. "	1.726	0.816	4.383	1.957
1000. "	1.823	0.922	4.555	2.188
2.mm	1.950	1.017	5.043	2.518
5."	1.273	0.753	5.015	2.548
10. "	0.3391	0.2640	2.293	1.452
20. "	0.0675	0.0632	0.5101	0.4470
33. "	0.0193	0.0188	0.1482	0.1408

Table 4

MASS EXTINCTION COEFFICIENTS FOR HAZE, CLOUDS, AND RAIN
(γ_{ex} in Neper km^{-1} per gm^{-3} liquid water content)

λ	Haze L $w=1.167 \cdot 10^{-5}\ gm^{-3}$	Cloud C.1 $w=0.06255\ gm^{-3}$	Cloud C.5 $w=0.2969\ gm^{-3}$	Rain-10 $w=0.5091\ gm^{-3}$
($\lambda \to 0$)	(3117.)	(250.1)	(142.8)	(2.573)
16.6μm	247.6			
17.0 "		257.8	168.3	
100. "	(36.8)	43.01	69.72	2.816
200. "	(16.8)	15.56	18.92	2.950
337. "	(10.5)	9.293	9.932	3.097
500. "	(7.21)	7.301	7.527	3.243
1.mm	(3.87)	(3.87)	3.924	3.580
2. "	(1.60)	(1.60)	(1.60)	3.830

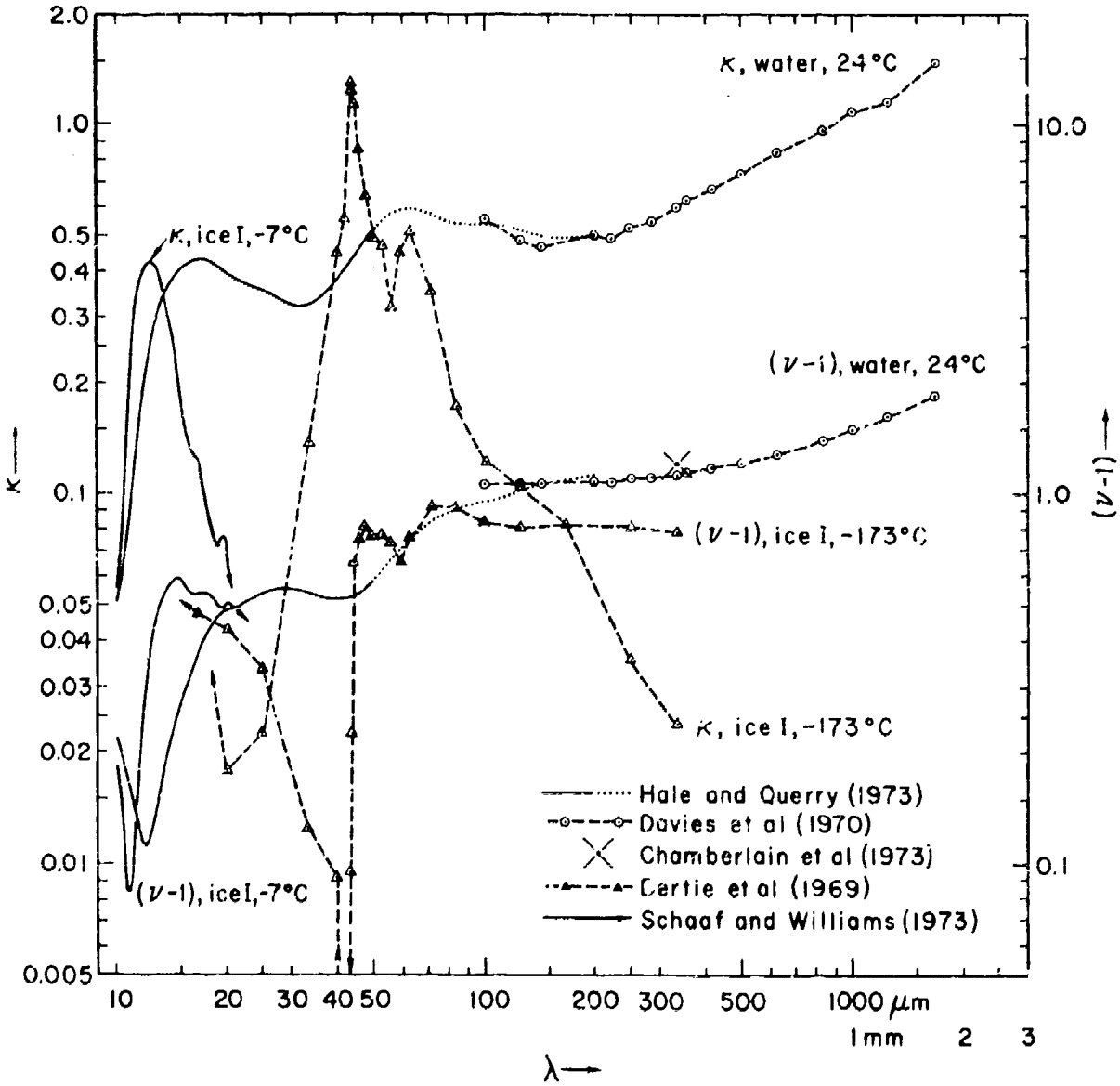

Fig. 1 - The optical constants of water according to recent measurements.

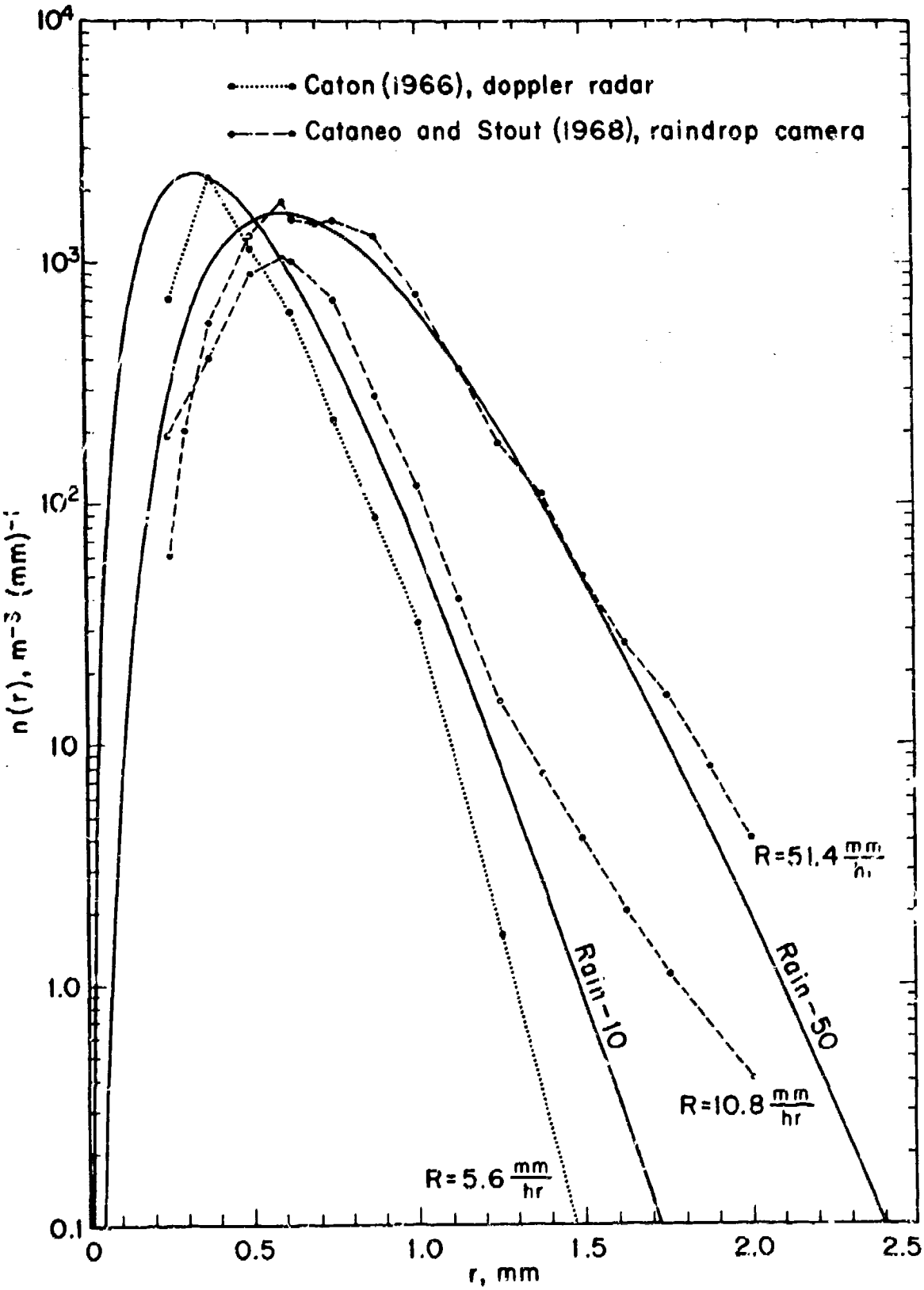

Fig. 2 - Adopted raindrop-size distribution models and some measurements.

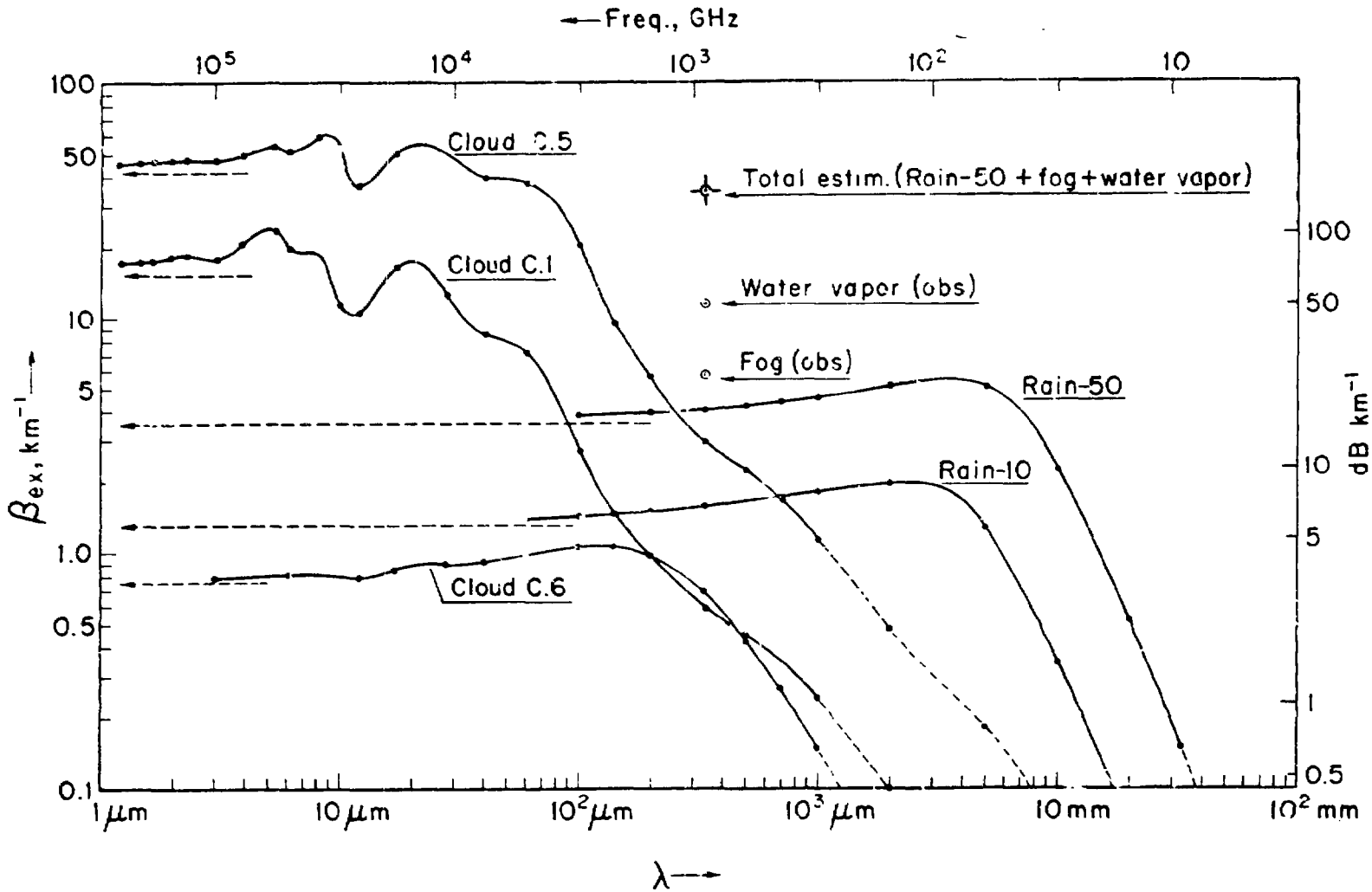

Fig. 3 - Theoretical cloud- and rain extinction coefficients excluding water vapor and other molecular absorption effects.

References

Battan, Louis, J., 1973: *Radar Observation of the Atmosphere.* University of Chicago Press, 324 pp.

Bertie, J. E., H. J. Labbé, and E. Whalley, 1969: Absorptivity of ice I in the range 4000-30 cm^{-1}. *J. Chem. Phys.*, 50, 4501-4520.

Birch, J. R., W. J. Burrows, and R. J. Emery, 1969: Observation of atmospheric absorption using submillimetre maser sources. *Infrared Physics*, 9, 75-83.

Burroughs, W. J., E. C. Pyatt, and H. A. Gebbie, 1966: Transmission of sub-millimetre waves in fog. *Nature*, 212, 387-388.

Button, Kenneth J. (ed.), 1974: Proceedings First International Conference on Submillimeter Waves and their Applications. *IEEE Trans. Microwave Theory Tech.*, MTT-22, 981-1120.

Cataneo, R., and Glenn E. Stout, 1968: Raindrop-size distributions in humid continental climates, and associated rainfall rate-radar reflectivity relationships. *J. Appl. Meteor.*, 7, 901-907.

Caton, P. G. F., 1966: A study of raindrop-size distributions in the free atmosphere. *Quart. J. R. Met. Soc.*, 92, 15-30.

Chýlek, Petr, 1973: Large-sphere limits of Mie-scattering functions, *J. Opt. Soc. Amer.*, 63, 699-706.

Davies, M., G.W.F. Pardoe, J. Chamberlain, and H. A. Gebbie, 1970: Submillimetre- and millimetre-wave absorption of some polar and non-polar liquids measured by Fourier transform spectroscopy. *Trans. Faraday Soc.*, 66, 273-292.

Deirmendjian, D., 1963a: Scattering and polarization properties of polydispersed suspensions with partial absorption. *Electromagnetic Scattering*. Pergamon Press, 171-189.

Deirmendjian, D., 1963b: *Complete Microwave Scattering and Extinction Properties of Polydispersed Cloud and Rain Elements*. Publication R-422-PR, The Rand Corp., 54 pp.

Deirmendjian, D., 1964: Scattering and polarization properties of water clouds and hazes. *Appl. Optics*, 3, 187-196.

Deirmendjian, D., 1965: Complete scattering and parameters of polydispersed hydrometeors in the λ0.1 to λ10 cm. range. *Radio Science*, 69D, 893-897.

Deirmendjian, D., 1969: *Electromagnetic Scattering on Spherical Polydispersions*. American Elsevier, 290 pp.

Deirmendjain, D., 1974: *Far Infrared and Submillimeter Scattering I. The Optical Constants of Water--A Survey*. Publication R-1486-PR, The Rand Corp., 19 pp.

Deirmendjian, D., R. Clasen and W. Viezee, 1961: Mie scattering with complex index of refraction. *J. Opt. Soc. Amer.* 51, 620-633.

Draegert, D. A., N.W.B. Stone, B. Curnutte, and D. Williams, 1966: Far infrared spectrum of liquid water. *J. Opt. Soc. Amer.*, 56, 64-69

Dudzinsky, S. J., Jr., 1974: *Atmospheric Effects on Terrestrial Millimeter-Wave Communications*. Publication R-1335-ARPA, The Rand Corp., 37 pp.

Fox, Jerome (ed.), 1971: *Proceedings of the Symposium on Submillimeter Waves*. Polytechnic Press, 726 pp.

Green, H. L. and W. R. Lane, 1964: *Particulate Clouds: Dusts, Smokes and Mists* (2nd ed.). Van Nostrand, 471 pp.

Hale, G. M., and M. R. Querry, 1973: Optical constants of water in the 200 nm to 200 μm wavelength region. *Appl. Optics*, 12, 555-563.

Hansen, J. E., 1971: Multiple scattering of polarized light in planetary atmospheres. Part II. Sunlight reflected by terrestrial water clouds. *J. Atmos. Sci.*, 28, 1400-1426.

Hansen, J. E. and J. W. Hovenier, 1974: Interpretation of the polarization of Venus. *J. Atmos. Sci.*, 31, 1137-1160.

Hulst, H. C. van de, 1957: *Light Scattering by Small Particles*. J. Wiley & Sons, 450 pp.

Kattawar, George W., and Gilbert N. Plass, 1975: Interior radiances in optically deep absorbing media-III. Scattering from haze L. *J. Quant. Spectrosc. Radiat. Transfer*, 15, 61-85.

Mason, B. J., 1971: *Cloud Physics* (2nd ed.). Clarendon Press, 671 pp.

Middleton, W.E.K., 1952: *Vision through the Atmosphere*. Univ. of Toronto Press, 250 pp.

Okita, T., 1961: Size distribution of large droplets in precipitating clouds. *Tellus*, 13, 509-521.

Penndorf, Rudolf B., 1962: Scattering and extinction coefficients for small absorbing and nonabsorbing aerosols. *J. Opt. Soc. Amer.*, 52, 896-904.

Platt, C.M.R., 1970: Transmission of submillimeter waves through water clouds and fogs. *J. Atmos. Sci.*, 27, 421-425.

Ray, S. P., 1972: Broadband complex refractive indices of ice and water. *Appl. Optics*, 11, 1836-1844.

Schaaf, J. W., and D. Williams, 1973: Optical constants of ice in the infrared. *J. Opt. Soc. Amer.*, 63, 726-732.

Thompson, B. D., and M. B. Wells, 1971: Scattered and reflected light intensities above the atmosphere. *Appl. Opt.*, 10, 1539-1549.

Wrixon, G. T., 1974: Measurements of atmospheric attenuation on an earth space path at 230 GHz using a sun tracker. In *Proc. 4th European Microwave Conference*, F. Gardiol (ed.), Microwave Exhibitions and Publishers Ltd., England, 222-226.